First-Principles Study on the Effects of Zr Dopant on the CO Adsorption on Ceria

Zongxian Yang,* Zhaoming Fu, Yanwei Wei, and Zhansheng Lu

College of Physics and Information Engineering, Henan Normal University, Xinxiang, Henan, 453007, People's Republic of China

Received: November 24, 2007; Revised Manuscript Received: July 17, 2008

With use of the first-principles density functional theory with the inclusion of the on-site Coulomb interaction of the Ce4f electrons (DFT+*U*) method, the adsorption of CO on the (110) surface of a stoichiometric $Ce_{0.75}Zr_{0.25}O_2$ system is studied systematically. It is found that, (1) in addition to the carbonate-like CO_3 structures, there exists a new adsorption species (a bent CO_2^- structure) on the $Ce_{0.75}Zr_{0.25}O_2(110)$ surface, and (2) the Zr-dopant can enhance the adsorption of CO and improve the CO oxidation process on the ceria surface by promoting the desorption of CO_2.

1. Introduction

Because of its particular redox property, ceria plays an important role in catalysis. Experimentally, it is found that lattice oxygen of the CeO_2 surface can react with CO by releasing CO_2 in the gas phase and leaving behind an O vacancy in the reducing conditions.[1] Here, CeO_2 acts as an oxygen buffer by releasing−uptaking oxygen through redox processes involving the Ce^{4+}/Ce^{3+} pair. First-principles calculations based on density functional theory (DFT) have been used to study the adsorption occurring on pure ceria.[2−4] Our previous work[2] studied the adsorption of CO on the ceria surfaces using the exchange and correlation functional (PW91) of Perdew et al.[5] and the all-electron projector-augmented wave (PAW) method of Blöchl,[6] and found that, for the adsorption of CO on the $CeO_2(110)$ surface, in addition to the weak adsorption sites, there exist two strong adsorption sites. In the strong adsorption sites, the CO molecule bridges two oxygen atoms and pulls these atoms out of their lattice sites, with the formation of $(CO_3)^{2-}$ species, and the CO−ceria bonding can be classified as chemisorption with adsorption energies of 0.76 and 1.95 eV/per CO, respectively, with the former (denoted as Ce-bridge in this paper and in the previous paper[2]) crossing the surface Ce-bridge and the latter (denoted as O-bridge) not. Recently, Nolan et al.[4] revisited the systems by including the on-site Coulomb interaction of Ce4f states using the DFT+*U* method.[7,8] In their study, only one strong adsorption site with the formation of a $(CO_3)^{2-}$ species corresponding to our Ce-bridge was reported, and they found that the adsorption is much stronger with an adsorption energy of 1.95 eV/per CO as compared with our GGA results (0.76 eV/per CO), showing the big effect of the DFT+*U* method on the adsorption energy. Both pervious studies[2,4] showed that only weak adsorption happened at the atop-O site on the pure $CeO_2(110)$ surface.

Much attention has been given to the study of the effects of Zr doping on the redox properties of CeO_2.[9−11] It has been found that the addition of ZrO_2 can increase oxygen release of CeO_2,[12] and the thermal stability of CeO_2 is greatly enhanced by mixing with zirconium oxide to form $Ce_xZr_{1-x}O_2$ solid solutions. Chemistry that occurs at the surfaces of ceria is critical in a variety of industrial applications, especially in catalysis. Therefore, research about the adsorption of CO on the surfaces of Zr-doped CeO_2 ($Ce_xZr_{1-x}O_2$) is of special interest. However, to our knowledge, there are very few first-principle studies for the adsorption of CO on Zr-doped ceria. In the present paper, we concentrate on investigating the effects of Zr doping through simulating the adsorption of CO on the $Ce_{0.75}Zr_{0.25}O_2(110)$ and $CeO_2(110)$ using the DFT+*U* method.[7,8] It is found that the Zr-dopant can enhance the adsorption of CO and may probably promote the desorption of CO_2 molecules from the surface. In addition, a new strong adsorption occurred at the atop-O site. These results reveal the important effects of Zr-doping on improving the reduction and catalytic properties of ceria.

The computational details are presented in Section 2. The calculated results are presented in Section 3, where the effects of Zr-doping are discussed by comparing the differences in atomic and electronic structures for undoped and Zr-doped CeO_2. A brief summary is given in Section 4.

2. Methodology

Spin-polarized Kohn−Sham density functional theory calculations were performed with use of the Vienna ab initio simulation package (VASP).[13−15] The electron exchange and correlation were treated within the generalized gradient approximation (GGA), using the Perdew−Burke−Ernzerhof (PBE) functionals. All systems studied here were treated with the DFT+*U* method,[7,8] since the regular DFT methods have been found to be unable to correctly describe the localization of cerium 4f states in partially reduced ceria. In the DFT+*U* method, a Hubbard parameter, *U*, is introduced for the Ce 4f electrons to describe the on-site Coulomb interaction; this helps to remove the self-interaction error and improves the description of correlation effects. Some authors have already described how the value of *U* is fitted against experimental results for correctly describing the properties of both the CeO_2 and partially reduced ceria (CeO_{2-x}).[16−18] It has been shown that by choosing an appropriate *U* parameter to account for the strong on-site Coulomb repulsion among the localized Ce 4f electrons, it is possible to consistently describe structural, thermodynamic, and electronic properties of CeO_2, Ce_2O_3, and CeO_{2-x}, which enables modeling of redox processes involving ceria-based materials.[16−18] Some studies have shown a linear dependency of the reduction energy of ceria as a function the effective parameter *U*.[19,20] It was pointed out that[20] the values of *U* presently used in the

* Author to whom correspondence should be addressed. E-mail: yzx@henannu.edu.cn.

10.1021/jp711154k CCC: $40.75
Published on Web 09/04/2008

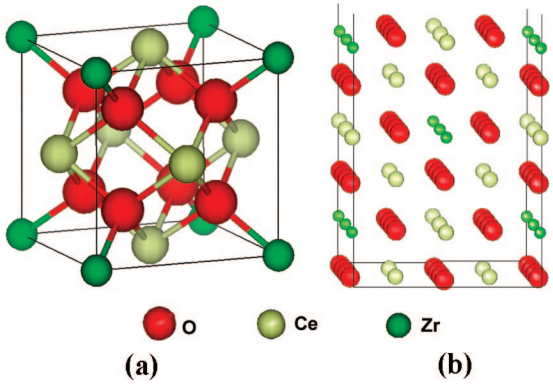

Figure 1. Optimized structural models of the systems studied in this paper: (a) the primitive cell of $Ce_{0.75}Zr_{0.25}O_2$ and (b) the side view of the $Ce_{0.75}Zr_{0.25}O_2(110)$-$(2\times1)$ surface. Here and in the following figures, yellow, red, green, and brown spheres represent the Ce, O, Zr, and C atoms, respectively.

literature ($U > 4$ eV) tend to overestimate the binding energy of CO to ceria surfaces, and the calculated adsorption energy for $U = 2$ eV is in good agreement with experimental results (2.27 eV[21]). In contrast, the energy for the complete CO oxidation reaction is effectively independent of U. However, the results of our test calculations and previous work[16−18] both indicated that only if $U = 5$ eV and greater can the localization of the Ce4f electrons in the partially reduced ceria be properly described. Therefore, a proper theoretical description of the interaction between CO and ceria surfaces is still under debate.[20] Considering that the focus of this paper is to study the effects of Zr dopants on the CO adsorption on ceria, the difference of adsorption energies (ΔE_{ad}, which is proved to be little dependent on the U value) between doped and undoped adsorption systems is more meaningful. Therefore, in all the calculations, we fixed the U value at 5 eV. Recently, Da Silva et al.[22] applied hybrid functionals to the rare-earth oxides (including ceria) and correctly predicted Ce_2O_3 to be an insulator as opposed to the ferromagnetic metal predicted by the local spin density (LDA) and generalized gradient (GGA) approximations. The adsorption of CO on the $CeO_2(110)$ surface has been studied by using hybrid density functional theory (DFT) in the form of the B3LYP functional.[23] The calculated adsorption energy (~2.1 eV) on the O-bridge site of $CeO_2(110)$ is close to the experimental value of 2.27 eV.[21] This shows another possibility of using hybrid functionals (other than the DFT+U method used here) to reduce the improper self-interaction.

The cerium 5s, 5p, 5d, 4f, 6s electrons, the 2s, 2p electrons of oxygen and carbon, and the zirconium 4s, 4p, 5s, 4d electrons were treated as valence electrons. The projector augmented wave (PAW) method is used to describe the effect that the ion core imposes on the valence electrons. The Kohn−Sham orbitals were expanded in plane waves with a kinetic energy cutoff of 30 Ry, and a minimum k-point density in each direction of 0.15 $Å^{-1}$. The Brillouin-zone integrations were performed by using a Gaussian smearing of SIGMA = 0.2 eV. The final results were extrapolated to that of SIGMA = 0 eV.

A primitive cell of ceria doped with 25% of Zr ($Ce_{0.75}Zr_{0.25}O_2$), shown in Figure 1a, was optimized with respect to both the cell parameter and the atomic positions until the force on each atom was less than 0.02 eV/Å and the stress tensor on the cell was less than 0.1 GPa. The calculated lattice constant is 5.42 Å, which is in agreement with the previous theoretical value (5.39 Å).[24] For the pure ceria, our calculated lattice constants, as well as the previous experimental and theoretical values in the literatures,[25−27] are given in Table 1. The $Ce_{0.75}Zr_{0.25}O_2(110)$-$(2\times1)$ surface shown in Figure 1b was cleaved from the optimized bulk cell. The surface was modeled by a supercell with a slab of finite thickness (11.6 Å, 6 atomic layers) separated by a vacuum layer that is sufficiently large (13 Å) to eliminate slab−slab interactions perpendicular to the surface, and the bottom 2 atomic layers were fixed at their bulk positions. Test calculations with a thicker vacuum layer (18 Å) showed that the calculated results are actually converged with respect to the vacuum thickness, e.g., the adsorption structures (C−O distances) are almost the same, the DOS have no obvious differences, and the total energies of the supercells have very small differences (<0.1 eV). The CO molecule was positioned 2 Å above a number of trial positions (e.g., atop-O, O-bridge, Ce-bridge, Ce−Zr-bridge, etc.) with its bond perpendicular to and its C-moiety toward the surface. The (2×1) surface unit cell was applied to eliminate interactions between CO adsorbates. The leading errors induced by the existence of dipole moment in the supercells were corrected by using the methods as implemented in the VASP.[13−15]

TABLE 1: The Calculated Lattice Constant of the Bulk CeO_2[a]

	exptl	theoretical	this work
lattice constant /Å	5.41 (ref 25)	5.49 (ref 26) 5.48 (ref 27)	5.48

[a] The previous experimental and theoretical values in the literatures are also shown for comparison.

The free CO and CO_2 molecules were simulated by using a large unit cell with dimensions of $8 \times 8 \times 10$ $Å^3$. The calculated equilibrium bond lengths of CO and CO_2 are 1.18 and 1.20 Å; the experimental values are 1.13 and 1.16 Å, respectively.[28,29] The calculated intramolecular binding energies [defined as $E_b = E_{atoms} - E_{mol}$, where E_{mol} and E_{atoms} are the ground-state energy of the molecule and the sum of total energies of its component atoms calculated by using unit cells of the same size] of CO and CO_2 are 258.9 and 202.5 kcal/mol, respectively, in good agreement with the experiment values of 259 and 191.2 kcal/mol.[30]

Vibrational frequencies for the adsorbed CO were computed through numerical differencing of the forces to generate a second derivative matrix. Diagonalization of the mass weighted matrix gave rise to vibrational frequencies and atomic displacements.

3. Results and Discussion

In this section, the adsorption properties and nature of the interaction (geometry, energetics, and electronic properties) are addressed.

3.1. Adsorption Geometries and Energetics. The binding strength of a CO molecule on the surface is quantified by the adsorption energy (E_{ad}), which is defined as

$$E_{ad} = E(\text{surface}) + E(CO_g) - E(\text{CO/surface}) \qquad (1)$$

where E(CO/surface) and E(surface) are the total energies of the surface with and without a CO adsorbate, and $E(CO_g)$ is the calculated total energy of a free CO molecule in the gas phase. The calculated adsorption energies of a CO in the optimized structures on $Ce_{0.75}Zr_{0.25}O_2(110)$ are listed in Table 2 and the E_{ad} values for CO on the $CeO_2(110)$ are also shown in the table for comparison. Similar to the adsorption nature of a CO on $CeO_2(110)$, it is found that there exist both weak and strong interactions for CO adsorption on $Ce_{0.75}Zr_{0.25}O_2(110)$. The weak interaction at the atop-cation (Ce^{4+} and Zr^{4+}) sites is

TABLE 2: The Optimized Adsorption Geometries and the Corresponding Adsorption Energies (E_{ad}, in eV) for a CO on $Ce_{0.75}Zr_{0.25}O_2$(110) and CeO_2(110)

Adsorption geometries	$E_{ad}[Ce_{0.75}Zr_{0.25}O_2]$	$E_{ad}[CeO_2]$
atop-O	1.01	0.43
O-bridge		
tilted	4.10	3.70
upright	4.00	3.00
Ce−Zr(Ce)-bridge		
tilted	3.16	2.15
upright	unstable	2.12
atop-Ce	0.21	0.18
atop-Zr	0.27	

also physisorption in nature, while the strong interaction sites have different features as compared with those on CeO_2(110). We will discuss the strong adsorptions in detail.

For the adsorption of a CO molecule on $Ce_{0.75}Zr_{0.25}O_2$(110), both an upright (Figure 2a) and a tilted configuration (Figure 2b) are found at the *O-bridge* site with the latter more stable, so the former corresponds to a metastable state. At the *Ce−Zr-bridge* site the adsorption is converged to a tilted configuration (Figure 2c). The adsorption energies are 4.00 (upright at the *O-bridge* site), 4.10 (tilted at the *O-bridge* site), and 3.16 eV (tilted at the *Ce−Zr-bridge* site). The adsorptions are clearly stronger on $Ce_{0.75}Zr_{0.25}O_2$(110) as compared with those on the CeO_2(110) surface, where the adsorption energies are 3.70 eV (3.00 eV) at the *O-bridge* site and 2.15 eV (2.12 eV) at the *Ce-bridge* site (the values in parentheses denote the adsorption energy for the metastable upright configurations). From parts a, b, and c in Figure 2, we can easily see that, at both *bridge* sites, two surface O atoms were drawn up a lot from the surface. For the *O-bridge* site, the distances of the C atom to the two surface O atoms is 1.36 Å, and there is an appreciable elongation of the intramolecular C−O bond length, which increased from 1.18 Å in a free CO to 1.24 Å in the adsorbed CO (Figure 2b). The adsorbed CO molecule bonds to two surface oxygen ions and forms a $(CO_3)^{2-}$ carbonate-like (planar) fragment with the CO bond tilting from the surface normal by 53.8°, as found on pure CeO_2(110). Similar structural changes were found for the CO molecule at the *Ce−Zr-bridge* site, where the distances of the C atom to two surface O atoms are 1.34 Å and the intramolecular CO bond length is elongated by 0.11 Å (Figure 2c). The angle between the intramolecular C−O bond and the surface normal is 57.0°. The structural changes induced by CO adsorption on the $Ce_{0.75}Zr_{0.25}O_2$(110) surface are larger than those on pure CeO_2(110).

It is known from the previous literatures[2,4] that the *atop-O* site is a very weak adsorption position for CO on pure ceria (CeO_2). But here on the $Ce_{0.75}Zr_{0.25}O_2$(110) surface, a strong adsorption arose at the atop-O site (cited as "*atop-O* site" in the following). At this site, the calculated adsorption energy is 1.01 eV, which is much larger than that on the pure CeO_2(110) surface (0.43 eV). Obviously, the former belongs to chemisorption, and the latter belongs to physisorption, showing that the Zr-doping enhances the adsorption very much at this site. Though it is not, by far, the most stable adsorption as compared with the $(CO_3)^{2-}$ configuration (E_{ad} = 4.10 eV, 3.16 eV), the presence of the new strong adsorption indicated that the Zr doping can affect the redox of ceria.

At this *atop-O* adsorption site, a surface O atom was pulled out from the $Ce_{0.75}Zr_{0.25}O_2$(110) surface by the CO adsorbate, resulting in a bent CO_2 species floating on the surface with an oxygen vacancy left behind in the surface. The adsorbed CO_2 species is similar to a free CO_2 molecule, but with a bent structure and stretched bond lengths because of the interaction with the surface: the C−O bond lengths are 1.27 and 1.26 Å, respectively, and the O−C−O angle is 136° (Figure 3a,b). We will further show in section 3.2 that the CO_2 species is negatively charged with an extra electron.

3.2. Electronic Structure and Stretching Frequencies. To understand the nature of the adsorption, the electronic structure will be studied, focusing on the total density of states (TDOS) and partial charges analysis for the strong adsorption sites.

As discussed in section 3.1, strong adsorption sites with the formation of a carbonate-like, $(CO_3)^{2-}$, structure at the *O-bridge* and the *Ce−Zr-bridge* sites exists on the $Ce_{0.75}Zr_{0.25}O_2$(110) surface. The Bader-type analysis[31] gave that there are totally about 23.6 (23.5) valence electrons on the adsorbed CO_3 species at the *O-bridge* (*Ce−Zr-bridge*) sites, in contrast to those expected for free CO_3 (22 electrons). Therefore, the CO_3 species are negatively charged with 1.6 (1.5) excess electrons, similar to the carbonate-like species (i.e., the $(CO_3)^{2-}$ with a formal charge of −2) found on the pure CeO_2(110) surface, which has been discussed in detail in previous papers.[2−4] The adsorption of CO drew up two surface O atoms (retaining about 0.8 electron each) from the surface, which can be depicted as $CO + 2O^- \rightarrow (CO_3)^{2-}$. Correspondingly, the substrate was partially reduced due to the leaving of O^- anions and the formation of oxygen vacancies in the surface. In each case, it is found that the 4f states of the two Ce cations (Ce^{4+}) neighboring the oxygen vacancies on the surface got excess electrons (about one electron for each Ce^{4+}) and reduced to Ce^{3+}.

The new adsorption structure at the "*atop-O* site" reflects the influence of Zr dopants although it is not the most stable one. Therefore we will investigate its electronic structure in detail. The TDOS for the "*atop-O* site" is shown in Figure 4. The TDOSs for an unreduced substrate, a free CO_2, and a reduced $Ce_{0.75}Zr_{0.25}O_2$(110) substrate with an oxygen vacancy on the surface are also shown in the figure for comparison. The TDOS in the "*atop-O* site" as shown in Figure 4a has the typical peak structure of the TDOS for the unreduced $Ce_{0.75}Zr_{0.25}O_2$(110) substrate (Figure 4b) with some additional small peaks in the gaps. Inspecting the TDOSs shown in Figure 4c,d, it is found that the TDOS in the "*atop-O* site" has an overall structure of the superposition of the TDOSs of a free CO_2 (Figure 4c) and a reduced $Ce_{0.75}Zr_{0.25}O_2$(110) substrate (Figure 4d). The TDOS curves for the "*atop-O* site" (Figure 4a) have two small peaks in the energy gap near the Fermi level. It is found that the small peak with the solid curve just below the Fermi level (spin up channel) is from the reduced substrate and contains only about one electron localized on one of the Ce cations on the surface neighboring the oxygen vacancy. In contrast, the other peak with the dashed curve (the spin down channel) lies across the Fermi level and is found to be from the bent CO_2 species (Figure 3b), suggesting that there exist unpaired electrons in the bent CO_2 species. However, it is known that there is no unpaired electron for a CO_2 molecule in the gas phase. Indeed, the integrated Bader charge[31] for the carbon and oxygen atoms contained in the bent CO_2 species gives 16.8 valence electrons in total, showing that the bent CO_2 species is charged with about one more electron as compared with the number of valence electrons (16) for a free CO_2. Therefore, when an O ion was pulled out by the CO adsorbate from the surface, it retained one electron as O^- and combined with the CO adsorbate to form CO_2^-, which can be depicted as $CO + O^- \rightarrow CO_2^-$. This is consistent with the fact that only one excess electron existed and localized on one of surface Ce cations in the substrate after the CO adsorption at the "*atop-O* site". The bent CO_2^- structure

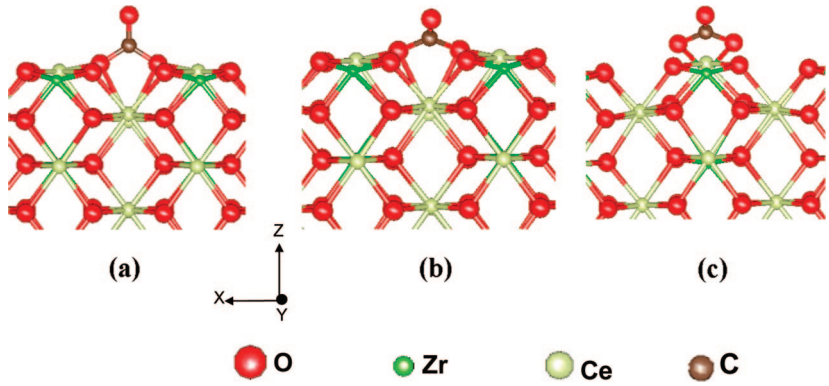

Figure 2. Optimized structures of CO adsorbed on $Ce_{0.75}Zr_{0.25}O_2(110)$ surface: (a) the upright configuration at the O-bridge site, (b) the tilted configuration at the O-bridge site, and (c) the tilted configuration at the Ce−Zr-bridge site.

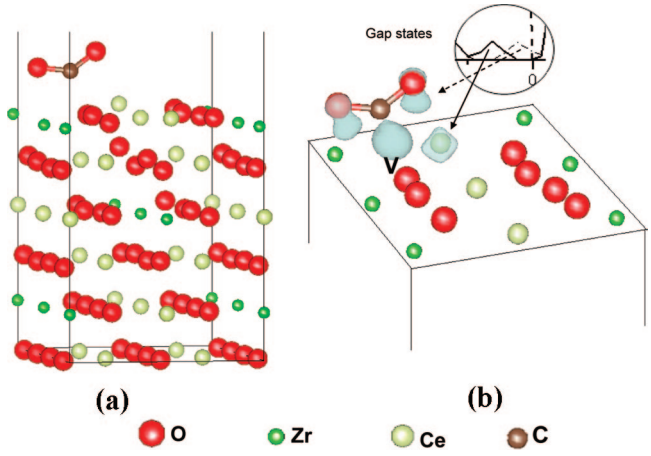

Figure 3. Optimized geometry structure (a) and the localized electron distribution (b) for CO adsorption at the atop-O site. The inset circle in part b shows the enlarged picture of the gap states near the Fermi level as shown in Figure 4a.

was also reported by previous studies.[32,33] For example, ab initio studies[33] for the absorption of CO_2 on the transition metals showed that one electron was transferred into CO_2 resulting in a bent CO_2^- structure with a O−C−O angle of about 133°, which is similar to our CO_2^- structure on $Ce_{0.75}Zr_{0.25}O_2(110)$, which has a O−C−O angle of 136°.

The stretching frequencies of a molecule can reflect the interaction intensity of atoms, and we can also deduce the molecule configuration from the vibrational modes. It is found that the vibrational modes of the bent CO_2^- species are similar to those of a free CO_2, indicating that, indeed, the new adsorption species has a CO_2-like structure. For a free CO_2, the calculated stretching frequencies of various vibrational modes are 2437 (an antisymmetric straight mode), 685 (a bent mode), and 1048 cm^{-1} (a symmetric straight mode), in good agreement with the experimental values (2349 and 667 cm^{-1}, the symmetric vibration is not observable by experiment because the dipole moment is zero). All stretching frequencies of the bent adsorbed CO_2^- species are smaller than the values of their corresponding modes for a free CO_2 except for the symmetric vibration frequency, which has a blue shift of 225 cm^{-1}.

In addition, the stretching frequencies of CO at all sites are calculated and given in Table 3. It is found that there are various vibrational modes observed for CO adsorbed at the O-bridge and the Ce−Zr-bridge sites. All strong adsorptions correspond to red shifts with the C−O bond lengths elongated, while for the weak interactions at the cation sites (i.e., the *atop-Zr* site and *atop-Ce* site), the CO stretching frequencies increase with the C−O bond lengths shrinking.

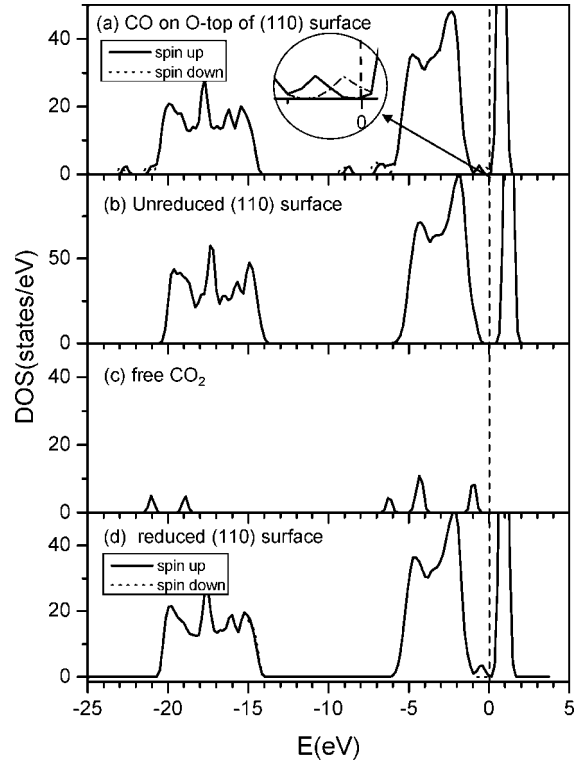

Figure 4. The density of states (DOS) for (a) CO on the O-atop site of $Ce_{0.75}Zr_{0.25}O_2(110)$ surface, (b) unreduced $Ce_{0.75}Zr_{0.25}O_2(110)$, (c) free CO_2, and (d) reduced $Ce_{0.75}Zr_{0.25}O_2(110)$ surface. For the unreduced $Ce_{0.75}Zr_{0.25}O_2(110)$ and the free CO_2, only the nonspin-polarized total DOSs are shown, since no spin-polarizations are found. For CO/$Ce_{0.75}Zr_{0.25}O_2(110)$ and the reduced $Ce_{0.75}Zr_{0.25}O_2(110)$ surface systems, DOSs for both the majority spin (solid lines) and minority spin (dashed lines) are shown. The vertical dot-dashed line at $E = 0$ eV represents the Fermi energy.

3.3. The Mechanism on the Effects of the Zr Dopant. The effects of the Zr dopant can be understood at the electronic level. To this end, the DOSs of the (110) surfaces of the unreduced CeO_2 (not shown in this paper) and $Ce_{0.75}Zr_{0.25}O_2$ (Figure 4b) are calculated. However, we find that Zr-doping does not induce any gap states, which is different from the noble metal doping.[34]

When partially reduced, the ceria surfaces retain some excess electrons left by the departing oxygen atoms. As shown above, at the strong adsorption sites (the *O-bridge* or the *Ce−Zr-bridge* sites), the CO adsorbate drew up two lattice oxygen atoms from the surfaces and left the surface partially reduced. The distribution of these excess electrons for all strong adsorption sites is calculated and shown in Figure 5. It is found that the excess

TABLE 3: The Calculated Stretching Frequencies of CO at Different Adsorption Sites[a]

adsorption geometries	ω (cm^{-1})
free CO	2150
atop-O	1787
O-bridge (tilted)	1552, 1154, 717, 604
Ce−Zr(Ce)-bridge (tilted)	1589, 1178, 682, 623
atop-Ce	2342
atop-Zr	2299

[a] The frequency of a free CO molecule in gas phase is also shown for comparison.

electrons are localized on two or four Ce cations near the adsorption sites depending on the final configurations. There exists a clear correlation between adsorption energies and the localization of the excess electrons.

First, we investigate the strong adsorption on pure CeO_2(110). For the metastable upright configuration at the *O-bridge* site (Figure 5a), the excess electrons are localized on four Ce cations, which can be viewed as two close pairs (Ce1−Ce2 and Ce3−Ce4). There are about 0.5 electron on each Ce atom. The E_{ad} increases from 3.00 eV (upright) to 3.70 eV (tilted) as the bridging carbonates become tilted (Figure 5b). Correspondingly, the excess electrons are redistributed and localized on one distant pair of Ce cations (Ce1−Ce3) because of the broken symmetry induced by the tilting of CO. Here, we can use the classical Coulomb potential to describe roughly the interaction of the localized electrons as shown in Figure 5a,b:

$$V_{\text{upright}} = 2 \times \frac{1}{4\pi\varepsilon_0}\left(\frac{0.25e^2}{r_1} + \frac{0.25e^2}{r_2} + \frac{0.25e^2}{\sqrt{r_1^2 + r_2^2}}\right) \quad (2)$$

$$V_{\text{tilted}} = \frac{1}{4\pi\varepsilon_0}\frac{e^2}{r_1} \quad (3)$$

Obviously, the V_{upright} is much larger than V_{tilted} according to eqs 2 and 3.

At the *Ce-bridge* site, the excess electrons are found to be localized on one close pair of Ce cations with a lower E_{ad} of 2.12 eV (metastable upright configuration) (Figure 5c). Though the tilting of CO can also break the symmetry to some extent (Figure 5d), the adsorption energy is only slightly changed (by 0.03 eV), since the localization of the excess electrons is not changed by the tilting. These results suggest that the excess electrons prefer residing on distant Ce cation pair(s) (e.g., the Ce_1−Ce_3 pair), which can lower the coulomb repulsion between the localized excess electrons and results in a higher E_{ad}. The coulomb repulsion effects can be seen clearly from the structure changes around the adsorption site. The distances between the Ce cations that accommodate excess electrons become larger as compared with the corresponding distances on the clean CeO_2(110) surface (Figure 5e) due to the coulomb repulsion.

Second, to clarify the mechanism about the Zr-doping effects on enhancing the CO adsorption, we study the excess electrons distribution in the strong adsorption configurations of CO on the $Ce_{0.75}Zr_{0.25}O_2$(110) surface. The upright configuration at the *O-bridge* site has an adsorption energy of 4.0 eV (Figure 5f), which is higher by 1.0 eV as compared with that on CeO_2(110). It is found that, at this site, the excess electrons are localized on one distant pair of Ce cations, which is different from that on CeO_2(110) (Figure 5a). The tilting of CO at this site has only very small effects on the adsorption energy (enhancing by 0.1 eV) (Figure 5g), since no obvious change in the excess electrons distribution is induced by the tilting of CO. At the *Ce-bridge* site, Zr-doping effects can be seen clearly. The Zr-doping modifies the excess electron distribution, by shifting the localization from a close pair (Figure 5d) to a distant pair of Ce cations (Figure 5h), resulting in a stronger adsorption. This might be one of the major reasons why Zr doping leads to the largest enhancement for the CO adsorption (ΔE_{ad} = 1.01 eV) at the Ce-bridge site, and suggests that the excess electron localization plays an important role in determining the adsorption strength of CO on the ceria (110) surface. On the other hand, as discussed previously,[34] when the ceria systems are partially reduced, some of the Ce^{4+} cations are reduced to Ce^{3+} ions. Because of their size difference (e.g., the radii of Zr^{4+}, Ce^{4+}, and Ce^{3+} are 0.84 Å, 0.97 Å and 1.19 Å, respectively[35]), the bigger Ce^{3+} ions may introduce strain to the lattice and increase the lattice energy. The smaller Zr dopants can spare some space to accommodate the bigger Ce^{3+} cations to release the strain and lower the lattice energy.

Therefore, the effects of Zr dopants can be clarified as the following two aspects: on one hand, the unreducible Zr^{4+} ions cannot "accept" excess electrons and, therefore, lead to the modification of the excess electrons distribution, which is different from the reducible Ce^{4+} ions. This modification tends to increase the distance of two localized electrons and lowers the Coulomb repulsion between them. On the other hand, the Zr dopant, with its smaller size, can lower the lattice energy through releasing the strain (induced by the partial reduction) in the substrate. It is the combination of the effects in the two aspects that results in the observed enhancement of the CO adsorption on the ceria (110) surface with Zr dopants.

Though the smaller Zr dopant can help to improve the redox properties of ceria, the redox ability of this CeO_2−ZrO_2 solid solution ($Ce_xZr_{1-x}O_2$) can be attributed completely to the reducible Ce ion. This suggests that there exists an optimal Ce/Zr ratio for the best catalytic effects.

3.4. The Enhancement of the CO Oxidation by Zr Doping and Discussion on the *U* Parameter. The desorption of CO_2 molecules from the (110) surface is a complicated process and is relevant in the practical CO oxidation process. In the following, we perform a preliminary analysis on the energetics, and try to find the possible effects of Zr doping in enhancing the CO oxidation on the ceria (110) surface.

The reaction (oxidation) processes of a CO molecule on the (110) surfaces of both CeO_2 and $Ce_{0.75}Zr_{0.25}O_2$ can be depicted as the following two steps:

The exothermic adsorption process:

$$\text{CO(g)} + 2\text{Ce}^{4+} + 2\text{O}^{2-} \rightarrow (\text{CO}_3)^{2-} + 2\text{Ce}^{3+} + 2(\text{O-vacancy})^* + E_{ad} \quad (4)$$

The endothermic desorption process of a CO_2:

$$2\text{Ce}^{3+} + (\text{CO}_3)^{2-} + 2(\text{O-vacancy})^* \rightarrow 2\text{Ce}^{3+} + \text{O}^{2-} + \text{CO}_2\text{(g)} + (\text{O-vacancy}) - E_{de} \quad (5)$$

where, (O-vacancy)* denotes the *partial* oxygen vacancy induced by the CO adsorption and the formation of CO_3 complex, (O-vacancy) denotes a *complete* oxygen vacancy left by the CO_2 desorption; the E_{ad} (adsorption energy) and E_{de} (desorption energy) correspond to the energies that are released (in the adsorption process 4) and absorbed (in the desorption process 5) in the reactions. We have a net exothermic effect for the (4) + (5) reactions with the positive reaction energies ($\Delta E = E_{ad} - E_{de}$) of 1.05 eV on the pure CeO_2(110) and 2.40 eV on the $Ce_{0.75}Zr_{0.25}O_2$(110) surface, indicating that the reaction processes are energetically favorable.

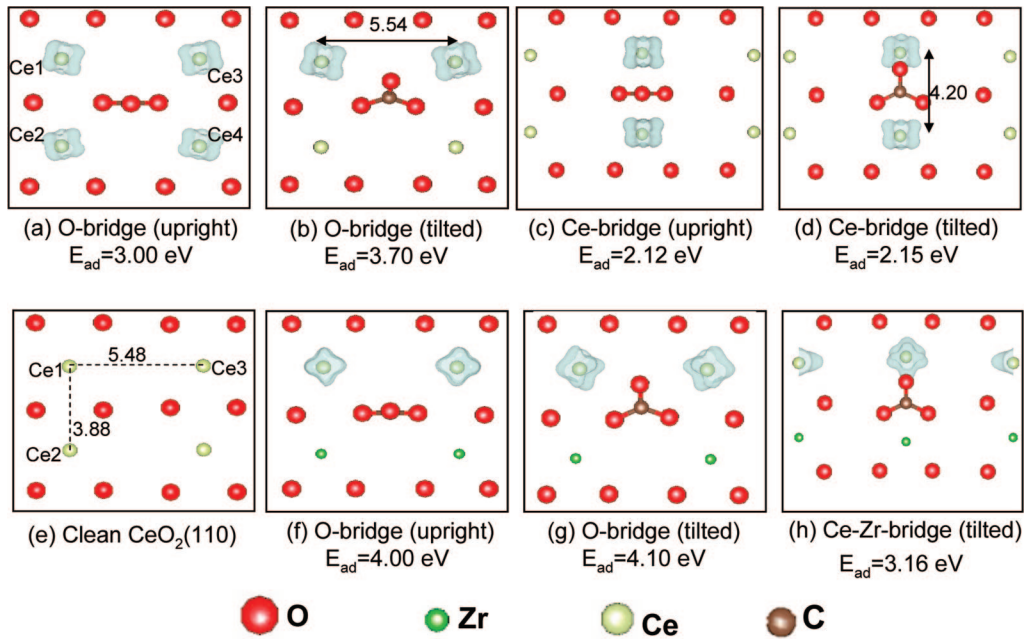

Figure 5. The top views of localized 4f electron distributions for different adsorption structures: (a−e) for $CeO_2(110)$ and (f−h) for $Ce_{0.75}Zr_{0.25}O_2(110)$. The isosurface value used is 0.05 e/Å^3.

TABLE 4: The Calculated Adsorption Energies of CO at O-Bridge Sites of $CeO_2(110)$ and $Ce_{0.75}Zr_{0.25}O_2(110)$ for Different U Parameters[a]

U parameter (eV)	E_{ad} (eV) CO/CeO_2	E_{ad} (eV) CO/$Ce_{0.75}Zr_{0.25}O_2$	$\Delta E_{ad} = E_{ad}(CO/Ce_{0.75}Zr_{0.25}O_2) - E_{ad}(CO/CeO_2)$
2	2.49	2.96	0.47
5	3.70	4.10	0.40

[a] The changes in the adsorption energy (ΔE_{ad}) induced by the Zr-dopant are also shown.

TABLE 5: The Calculated Desorption Energies of CO_2 for the O-Bridge Site Adsorption Systems: CO/CeO_2(110) and CO/$Ce_{0.75}Zr_{0.25}O_2$(110) for Different U Parameters[a]

U parameter (eV)	E_{ad} (eV) CO/CeO_2	E_{ad} (eV) CO/$Ce_{0.75}Zr_{0.25}O_2$	$\Delta E_{de} = E_{de}(CO/Ce_{0.75}Zr_{0.25}O_2) - E_{de}(CO/CeO_2)$
2	2.54	1.68	0.86
5	2.65	1.70	0.95

[a] The changes in the desorption energy (ΔE_{de}) induced by the Zr-dopant are also shown.

On the pure $CeO_2(110)$, the CO molecules react with the lattice O atoms to form carbonates with a large energy release [E_{ad} = 3.70 (*O-bridge*) and 2.15 eV (*Ce-bridge*) per CO]. Comparatively, the desorption of a CO_2 takes less energy [E_{de} = 2.65 (*O-bridge*) and 1.10 eV (*Ce-bridge*)]. In contrast, on the $Ce_{0.75}Zr_{0.25}O_2(110)$ surface, the adsorptions are enhanced with larger adsorption energies [E_{ad} = 4.10 (*O-bridge*) and 3.16 eV (*Ce−Zr-bridge*)], and the CO_2 desorption is promoted with less endothermic energies [E_{de} = 1.70 (*O-bridge*) and 0.80 eV (*Ce−Zr-bridge*)]. This might be an essential reason why Zr doping can improve the CO oxidation. The above analysis only showed that the reaction processes are energetically favorable. Actually, the CO oxidation process will be dominated by the activation energy. We will deal with this matter as well as the dynamitics properties of the desorption process in the future.

As mentioned in section 2, the reduction energy of ceria and the binding energy of CO to ceria surfaces depend on the effective parameter U.[19,20] As a test, we have studied the energetics of CO adsorption and CO_2 desorption on the O-bridge site of both $CeO_2(110)$ and $Ce_{0.75}Zr_{0.25}O_2(110)$ systems using different U parameters. The corresponding results are listed in Tables 4 and 5, where, E_{ad} and E_{de} are the adsorption energy of CO and desorption energy of CO_2, respectively, while ΔE_{ad} and ΔE_{de} are the quantities reflecting the changes in the adsorption and desorption energies induced by the Zr-dopant. The results suggest that the adsorption energy (E_{ad}) is strongly dependent on the U value, while the desorption energy (E_{de}) seems to be little dependent on U, in agreement with the conclusion of Huang et al.[20] Most importantly, the values of ΔE_{ad} and ΔE_{des} induced by the Zr doping are changed very little for different U values.

Although the DFT+U method is not perfect to depict the adsorption energy, it would be appropriate to use to describe the Zr-doping effects on the redox properties because the ΔE_{ad} and ΔE_{des} are roughly independent of the U value. As for the electronic structure, only if $U \geq 5$ eV can rational results (e.g., electron localization and the insulating feature of the reduced substrate) be obtained.

4. Conclusions

Using the DFT+U method, the adsorption of a CO molecule on the stoichiometric $Ce_{0.75}Zr_{0.25}O_2(110)$ surface is studied systematically. It is found that CO can be adsorbed strongly on both the $CeO_2(110)$ and $Ce_{0.75}Zr_{0.25}O_2(110)$ surfaces. The Zr dopants can enhance the CO adsorption and may promote the CO_2 desorption from the surface, and therefore, improve the CO oxidation process on the ceria surface. Besides, a new strong adsorption was found at the atop-O site with the formation of a CO_2^- configuration on the $Ce_{0.75}Zr_{0.25}O_2(110)$ surface.

The effects of Zr-doping are analyzed both electronically and geometrically. On one hand, the Zr doping can modify the distribution of the excess electrons in the reduced ceria and lower the Coulomb repulsion between them. On the other hand, the Zr dopant can lower the lattice energy through releasing

the strain in the reduced substrate. It is the combination of effects in the two aspects that result in the observed improvement of the CO oxidation on the ceria (110) surface with Zr dopants.

Acknowledgment. This work was supported by the National Natural Science Foundation of China (Grant No. 10674042) and the Henan Innovation Project For University Prominent Research Talents (HAIPURT: 2007KYCX004) of China.

References and Notes

(1) Trovarelli, A. *Catal. Rev. Sci. Eng.* **1996**, *38*, 439.
(2) Yang, Z.; Woo, T. K.; Hermansson, K. *Chem. Phys. Lett.* **2004**, *396*, 384.
(3) Nolan, M.; Parker, S. C.; Watson, G. W. *Surf. Sci.* **2006**, *600*, L175.
(4) Nolan, M.; Watson, G. W. *J. Phys. Chem.* **2006**, *110*, 16600.
(5) Perdew, J. P.; Chevary, J. A.; Vosko, S. H.; Jackson, K. A.; Pederson, M. R.; Singh, D. J.; Fiolhais, C. *Phys. Rev. B* **1992**, *46*, 6671.
(6) Bloechl, P. E. *Phys. Rev. B* **1994**, *50*, 17953.
(7) Anisimov, V. I.; Zaanen, J.; Andersen, O. K. *Phys. Rev. B* **1991**, *44*, 943.
(8) Dudarev, S. L.; Botton, G. A.; Savrasov, S. Y.; Humphreys, C. J.; Sutton, A. P. *Phys. Rev. B* **1998**, *57*, 1505.
(9) Yang, Z.; Woo, T. K.; Hermansson, K. *J. Chem. Phys.* **2006**, 124.
(10) Rodriguez, J. A. *Abstracts of Papers*; 229th ACS National Meeting, San Diego, CA, March 13−17, 2005; American Chemical Society: Washington, DC, 2005.
(11) Masui, T.; Imanaka, N. *Mater. Integr.* **2003**, *16*, 29.
(12) Campbell, C. T.; Peoden, C. H. F. *Science* **2005**, *309*, 713.
(13) Kresse, G.; Hafner, J. *Phys. Rev. B* **1993**, *47*, 558.
(14) Kresse, G.; Furthmuller, J. *Comput. Mater. Sci.* **1996**, *6*, 15.
(15) Kresse, G.; Furthmuller, J. *Phys. Rev. B* **1996**, *54*, 11169.
(16) Nolan, M.; Parker, S. C.; Watson, G. W. *Surf. Sci.* **2005**, *595*, 223.
(17) Nolan, M.; Grigoleit, S.; Sayle, D. C.; Parker, S. C.; Watson, G. W. *Surf. Sci.* **2005**, *576*, 217.
(18) Andersson, D. A.; Simak, S. I.; Johansson, B.; Abrikosov, I. A.; Skorodumova, N. V. *Phys. Rev. B* **2007**, *75*, 035109.
(19) Fabris, S.; Vicario, G.; Balducci, G.; de Gironcoli, S.; Baroni, S. *J. Phys. Chem.* **2005**, *109*, 22860.
(20) Huang, M.; Fabris, S. *J. Phys. Chem. C* **2008**, *112*, 8643.
(21) Breysse, M.; Guenin, M.; Claudel, B.; Veron, J. *J. Catal.* **1973**, *28*, 54.
(22) Da Silva, J. L. F.; Ganduglia-Pirovano, M. V.; Sauer, J.; Bayer, V.; Kresse, G. *Phys. Rev. B* **2007**, *75*, 045121/1.
(23) Herschend, B.; Baudin, M.; Hermansson, K. *Chem. Phys.* **2006**, *328*, 345.
(24) Rodriguez, J. A.; Hanson, J. C.; Kim, J.-Y.; Liu, G.; Iglesias-Juez, A.; Fernandez-Garcia, M. *J. Phys. Chem.* **2003**, *107*, 3535.
(25) Eyring, L. *Handbook on the Physics and Chemistry of Rare Earths*; Gschneider, K. A., Eyring, L., Eds.; North-Holland, Amsterdam, 1979; Vol. 3.
(26) Tibiletti, D.; Amieiro-Fonseca, A.; Burch, R.; Chen, Y.; Fisher, J. M.; Goguet, A.; Hardacre, C.; Hu, P.; Thompsett, D. *J. Phys. Chem.* **2005**, *109*, 22553.
(27) Skorodumova, N. V.; Baudin, M.; Hermansson, K. *Phys. Rev. B* **2004**, *69*, 075401/1.
(28) Chackeria, C., Jr *J. Chem. Phys.* **1976**, *65*, 4228.
(29) Cornaggia, C. *Phys. Rev. A* **1996**, *54*, R2555.
(30) Hammer, B.; Hansen, L. B.; Norskov, J. K. *Phys. Rev. B* **1999**, *59*, 7413.
(31) Henkelman, G.; Arnaldsson, A.; Jonsson, H. *Comput. Mater. Sci.* **2006**, *36*, 254.
(32) Freund, H.; Belmer, H.; Bartos, B. *Surf. Sci.* **1987**, *180*, 550.
(33) Freund, H.; Messmer, R. P. *Surf. Sci.* **1986**, *172*, 1.
(34) Yang, Z.; Luo, G.; Lu, Z. *J. Chem. Phys.* **2007**, *127*, 074704.
(35) Shannon, R. D. *Acta Crystallogr., Sect. A: Cryst. Phys., Diffr., Theor. Gen. Crystallogr.* **1976**, *A32*, 751.

JP711154K